Label-Free, Single-Molecule Detection with Optical Microcavities

Andrea M. Armani, *et al.*

Science **317**, 783 (2007);
DOI: 10.1126/science.1145002

Science (print ISSN 0036-8075; online ISSN 1095-9203) is published weekly, except the last week in December, by the American Association for the Advancement of Science, 1200 New York Avenue NW, Washington, DC 20005.

to symmetry-breaking device inhomogeneities introduced during fabrication.
24. M. L. Roukes, *Electron Devices Meeting, 2004. IEDM Technical Digest. IEEE International* (Institute of Electrical and Electronics Engineers, Piscataway, NJ, 2004) pp. 539–542.
25. M. C. Lonergan *et al.*, *Chem. Mater.* **8**, 2298 (1996).
26. D. Devoe, *Sens. Actuat. A* **88**, 263 (2001).
27. R. G. Beck, M. A. Eriksson, R. M. Westervelt, K. L. Campman, A. C. Gossard, *Appl. Phys. Lett.* **68**, 3763 (1996).
28. Y. Zhang, M. P. Blencowe, *J. Appl. Phys.* **92**, 7550 (2002).
29. R. Knobel, A. N. Cleland, *Appl. Phys. Lett.* **81**, 2258 (2002).
30. This work was supported by the Defense Advanced Research Projects Agency Microsystems Technology Office Micro Gas Analyzer through Department of Interior contract no. NBCH1050001. We thank W. van de Graaf and S. Degroote for the epitaxial crystal deposition and P. Van Dorpe and J. M. Choi for discussions.

Supporting Online Material
www.sciencemag.org/cgi/content/full/317/5839/780/DC1
Materials and Methods
SOM Text
Figs. S1 and S2
References

8 May 2007; accepted 6 July 2007
10.1126/science.1144793

Label-Free, Single-Molecule Detection with Optical Microcavities

Andrea M. Armani,[1] Rajan P. Kulkarni,[2] Scott E. Fraser,[1,2]* Richard C. Flagan,[3]* Kerry J. Vahala[1]

Current single-molecule detection techniques require labeling the target molecule. We report a highly specific and sensitive optical sensor based on an ultrahigh quality (Q) factor ($Q > 10^8$) whispering-gallery microcavity. The silica surface is functionalized to bind the target molecule; binding is detected by a resonant wavelength shift. Single-molecule detection is confirmed by observation of single-molecule binding events that shift the resonant frequency, as well as by the statistics for these shifts over many binding events. These shifts result from a thermo-optic mechanism. Additionally, label-free, single-molecule detection of interleukin-2 was demonstrated in serum. These experiments demonstrate a dynamic range of 10^{12} in concentration, establishing the microcavity as a sensitive and versatile detector.

Single-molecule fluorescence experiments have improved our understanding of many fundamental biological processes, such as protein folding kinetics (*1*), molecular transport (*2*, *3*), and aspects of DNA replication (*4*). However, all of these breakthrough experiments required labeling of the target molecule (*5*, *6*). In the case of surface-enhanced Raman spectroscopy (SERS), total internal reflection fluorescence microscopy (TIRF) and confocal microscopy, this label behaves as an amplifier for an otherwise undetectable single-molecule signal; however, it also restricts an experiment's scope, because there must be prior knowledge of the target's presence and the target molecule must be modified to incorporate the label (*7*–*12*). There have been several attempts to overcome this need to label the analyte by developing label-free sensing technologies, ranging from fiber-optic waveguides (*13*) and nanowires (*14*) to nanoparticle probes (*15*), biochips (*16*), and mechanical cantilevers (*17*), but none has achieved single-molecule sensitivity.

Optical microcavities have been proposed as a powerful method to achieve label-free detection of single molecules because the resonant recirculation of light within a microcavity allows the light to sample target molecules many more times (*18*–*21*). For example, in a simple optical waveguide sensor, the input light has only one opportunity to interact with the target molecule. In contrast, by using a planar microcavity with a quality (Q) factor of 10^8 (Fig. 1A), the molecule is sampled more than 100,000 times. This increased sampling manifests itself both as a shift of the resonant wavelength and as a decrease in the Q factor as the target molecules directly change the optical path length and/or the cavity loss of the sensor (*18*, *19*). The current work extends these ideas by adding a new mechanism through which molecules can induce a resonant wavelength shift. In particular, it will be shown that a thermo-optic mechanism greatly enhances detection sensitivity. Biochemically functionalizing the surface of the resonator to recognize the target molecule should provide an excellent platform for ultrasensitive detection and specific identification of dissolved, unlabeled target molecules (*22*, *23*).

We fabricated planar arrays of silica microtoroid whispering-gallery resonators (Fig. 1A) using a simple three-step process: (i) circular oxide pads were lithographically defined; (ii) the silicon wafer was selectively etched with xenon difluoride, forming arrays of silica microdisks; and (iii) the microdisks were reflowed with a CO_2 laser (*24*, *25*). Microtoroids offer Q factors in excess of 100 million for enhanced detection sensitivity, and their silica surfaces are readily functionalized for specific detection of biomolecules (*23*). The microtoroids were coupled to a tunable laser and detector by a tapered optical fiber waveguide and were immersed in water within a microaquarium with syringe inlets for introducing samples (*26*). The tapered optical fiber waveguide launches light into the whispering-gallery mode at the periphery of the microtoroid. The resonant whispering-gallery mode is partially confined inside the silica microtoroid, but it evanesces into the liquid environment (Fig. 1B). Thus, the light interacts strongly with the molecules once they are captured on the toroidal surface, in a manner similar to the way that a surface plasmon resonance (SPR) sensor interrogates a sample (*27*). The silica surfaces were sensitized either with biotin or antibodies to capture specific molecules [avidin or the target antigen, respectively (*26*)]. This binding interaction creates red shifts of the resonant wavelength that can be monitored in real time (*26*). In the static condition without the presence of biological molecules, the opposing thermo-optic

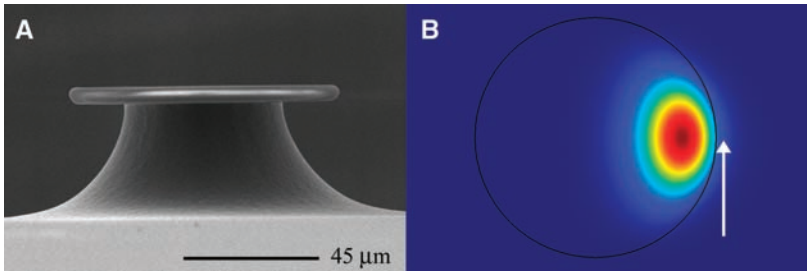

Fig. 1. The microtoroid resonator biological sensor. (**A**) A scanning electron micrograph (SEM) image of the UHQ microtoroid optical resonator. The silica microtoroid is fabricated on a silicon wafer using planar lithography and reflowed using a CO_2 laser. The typical microtoroid diameter used in this work was 80 μm. (**B**) A finite element model [FEMLAB (COMSOL, Burlington, Massachusetts, USA)] of a 4-μm minor diameter microtoroid resonator immersed in water. Although the majority of the optical field resides in the silica toroid, a portion of the field evanesces into the environment (indicated by a white arrow). The interaction of the whispering-gallery mode with the environment, specifically molecules bound on the surface of the toroid, enables the ultrasensitive detection.

[1]Department of Applied Physics, MC 128-95, California Institute of Technology, Pasadena, CA 91125, USA. [2]Division of Biology, MC 139-74, California Institute of Technology, Pasadena, CA 91125, USA. [3]Division of Chemistry and Chemical Engineering, MC 210-41, California Institute of Technology, Pasadena, CA 91125, USA.

*To whom correspondence should be addressed. E-mail: sefraser@caltech.edu (S.E.F.); flagan@caltech.edu (R.C.F.)

effects of water and of silica balance to stabilize the conventional thermally induced shift (*26*).

The working range of this device was determined with interleukin-2 (IL-2), a cytokine released in response to immune system activation to extrinsic and intrinsic stimuli. Concentrations ranging from 1×10^{-19} M to 1×10^{-6} M were controllably flowed past the microtoroid resonator using a syringe pump (*26*). For IL-2, the highest sensitivity occurred in the lower concentration range. The dose-response curve (Fig. 2) is sigmoidal, as would be expected from antibody-antigen binding if there were a finite number of binding sites. An easily detectable response was obtained at 5×10^{-18} M, with greater than 10:1 signal-to-noise ratio (Fig. 2, inset A). With increasing concentration, the responsivity diminished; however, wavelength shifts were detectable for concentrations as large as 10^{-6} M (Fig. 2, inset B). This working range is a 12-decade concentration range (10^{12}). This can be compared with that for other label-free room-temperature detection techniques, such as nanowire sensors (10^{3}) (*28*) and microcantilevers (10^{3}) (*29*) and is comparable to or greater than fluorescent or luminescent assays such as chemiluminescence (*30*).

For the lowest concentrations where shifts are observed, small numbers of molecules would be expected to interact with the toroid, which suggests that the sensor might accomplish label-free single-molecule detection. To investigate this regime further, a data acquisition system was used to measure resonant wavelength versus time at fixed concentrations and flow rates. Figure 3A shows shift responses versus time at three concentrations of IL-2 (*26*). By optimizing solution concentration, solution injection rate, and data acquisition rate, shifts caused by individual molecules binding to the surface of the toroid were resolved. We observed stepwise shifts, and their frequency scaled linearly with concentration. Using raw data like that presented in Fig. 3A, we plotted a histogram of the distribution of shifts over a given period of time for several concentrations of IL-2 (bin size is 0.001 pm) (Fig. 3C). In each case, the histogram has a maximum shift value that is independent of the concentration. This behavior is expected because wavelength shifts will depend on the strength of interaction between the bound molecule and whispering-gallery optical mode. The interaction will be strongest for binding at the equatorial plane and diminish rapidly as molecules bind even a few micrometers offset from this plane. Hence, these histogram plots are consistent with somewhat uniform binding of molecules over the toroid surface, thereby creating a distribution of shifts with a maximum given by molecules at the equatorial plane (*26*).

To further verify the single-molecule nature of these binding events, the statistics in time were studied in (*26*) and confirmed a Poissonian behavior for binding events. A single-molecule photo-bleaching experiment was also designed using a Cy5-labeled antibody (*31*). The experimental details and the results demonstrating single-molecule bleaching using the toroid as the excitation source are contained in (*26*).

The single-molecule shifts observed here are large based on previously proposed detection mechanisms (*18*, *19*). However, at the fundamental level, these theories assume that biological molecules have only a direct effect on either optical path length or Q factor by way of their complex polarizability. In such cases, it is straightforward to show that sensitivity scales linearly with microcavity Q factor and that wavelength shifts produced by single-molecule binding events are several orders of magnitude too small to explain the current observations. We propose instead, and verify through a series of measurements, a mechanism of detection that attains a greatly enhanced sensitivity by leveraging the high Q factor of the silica microtoroid twice (i.e., quadratic dependence of sensitivity with Q factor). This mechanism, not previously considered in a microresonator sensor, results when the high circulating intensities within the resonator locally heat molecules attached to the whispering gallery. This temperature increase results in a red shift of the resonant wavelength through the thermo-optic effect, when the whispering-gallery material itself (in this case, silica) is heated by the molecule. Contrasting this mechanism with the conventional method of microcavity detection based on directly induced changes in optical path length of the whispering-gallery resonant mode shows that the optical path length in the present case is varied indirectly and in proportion to the intensity-induced heating of the molecule. This mechanism therefore receives a double benefit (i.e., quadratic) from the ultrahigh Q factor (UHQ): first, from the narrow linewidth (i.e., improved resolution in measuring shifts), and second, from an increase in the intrinsic shift by way of the thermo-optic effect.

The expected thermo-optic wavelength shift is straightforward to predict. Beginning with the wave equation and adding a perturbing thermal contribution to the susceptibility, the theoretical wavelength shift produced by a single molecule (bound at the intensity maximum) by the thermo-optic mechanism can be shown to be given by (*32*):

$$\left[\frac{\delta\lambda}{\lambda}\right]_{SM} = \frac{\sigma\,\lambda\,^{dn}/_{dT}}{8\pi^2 n^2 \kappa V} QP \int \frac{|u(\boldsymbol{r})|^2}{|\boldsymbol{r}| + \varepsilon} d\boldsymbol{r} \qquad (1)$$

where λ is the wavelength, σ is the absorption cross section of the molecule, dn/dT is the optothermal constant of silica (1.3×10^{-5} K^{-1}), κ is thermal conductivity, n is the effective refractive index of the silica toroid, V is the optical mode volume, Q is cavity Q factor, and P is the coupled optical power. The integral in this expression accounts for the spatial overlap of the whispering-gallery mode field [u(r)], with the temperature profile created by the nearly pointlike molecular heat source. The parameter ε is on the order of the physical radius of the molecule (*33*) and, as shown below, has a negligible role in determining the magnitude of predicted shifts. As noted above, the strength of the thermo-optic effect depends on the circulating intensity within the toroidal whispering gallery, as evident in Eq. 1 by the dependence of the resonance shift on the coupled optical power, cavity Q, and modal volume.

Using this expression, we can establish the absorption cross section required to create a shift equal to one-cavity linewidth (*34*),

$$\sigma_1 = \frac{V}{Q^2}\frac{1}{P}\frac{8\pi^2 n^2 \kappa}{\lambda\,^{dn}/_{dT}}\left[\int \frac{|u(\boldsymbol{r})|^2}{|\boldsymbol{r}| + \varepsilon} d\boldsymbol{r}\right]^{-1} \qquad (2)$$

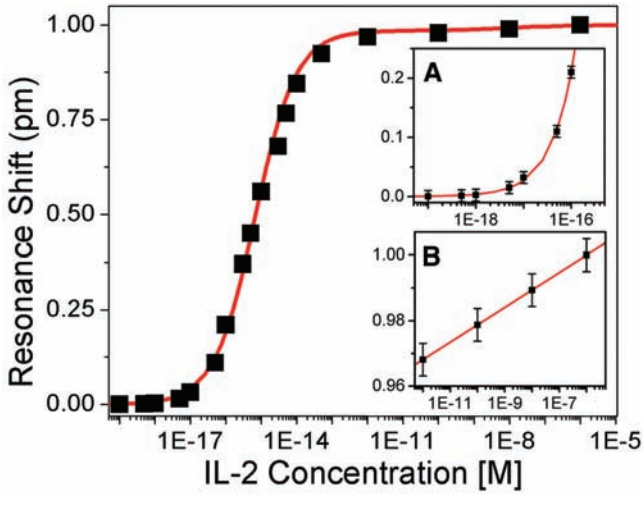

Fig. 2. The working range and dose response of the microtoroid sensor was investigated using a series of IL-2 solutions ranging from 10^{-19} M to 10^{-6} M. The Q of the cavity used in this study was 1.83×10^{8}. This response is sigmoidal, as would be expected from antibody-antigen binding if there were a finite number of binding sites. The first reliable signal was obtained at 5×10^{-18} M. The total working range of the sensor is from 5 aM (5×10^{-18}) to 1 μM (1×10^{-6}); the response of the sensor is not linear over this entire concentration range. The error bars are smaller than the symbols in the main graph and are shown in the insets. (**A**) Enlarged view of the low concentration response. The first concentration that has a detectable response is 5 aM. The error in this data is ± 0.005 pm. (**B**) Enlarged view of the higher concentration response (after considerable site saturation has occurred). The error in this data is ± 0.005 pm.

This figure of merit illustrates how the sensitivity benefits quadratically from the cavity Q factor. As an example, for a cavity Q factor of 250 million, a coupled power of 1 mW, a molecular radius in the range of 3 to 50 nm (*34*), a wavelength of 680 nm, a toroid of diameter 80 μm, and the optical and thermal constants of silica, σ_1 is between 1.1×10^{-17} cm^2 and 1.5×10^{-17} cm^2. This value is well below the values for many biomolecules and does not represent a fundamental limit of detection because, in principle, detection of sub-linewidth shifts is possible provided that the signal-to-noise ratio is adequate (*34*). Conversely, if a cross section of 2×10^{-16} cm^2 is assumed (typical of several molecules used in this study), then a single-molecule wavelength shift of between 50 and 33 fm is predicted, which is easily detected for a UHQ microcavity. We note that the thermo-optic mechanism is not limited to UHQ silica resonant cavities and can be generalized to other lower-Q resonant cavities, provided that power levels are substantially boosted to overcome the reduced Q.

We verified the proposed thermo-optic detection mechanism and investigated its universality by performing a series of single-molecule detection experiments using molecules of varying absorption cross sections, ranging from 10^{-16} to 10^{-13} cm^2 at low concentrations (*35*). The dependence of the resonant shift on Q was verified by using cavities with Q factors of either $\sim 1 \times 10^8$ or $\sim 2 \times 10^8$ (*26*). The lowest cross section molecules used were the IL-2 antigen (Fig. 3), protein G, and streptavidin. Two different polyclonal antibodies were also used and served as intermediate absorption cross section molecules. Two high–cross section fluorescent dye molecules were also used: Cy5-labeled antibody (fluorescent dye) and QSY-21 (a quencher molecule designed to absorb light like a fluorescent dye but not to re-emit photons) to provide further cross-sectional dynamic range in the test. If we assume that the largest shift in the histogram corresponds to the case of a single-molecule binding event at the region of highest intensity (i.e., the equatorial plane of the whispering gallery), this maximum shift can be plotted versus the molecular cross sections to verify Eq. 1.

Figure 4 summarizes the theoretical predictions and experimental results by plotting the

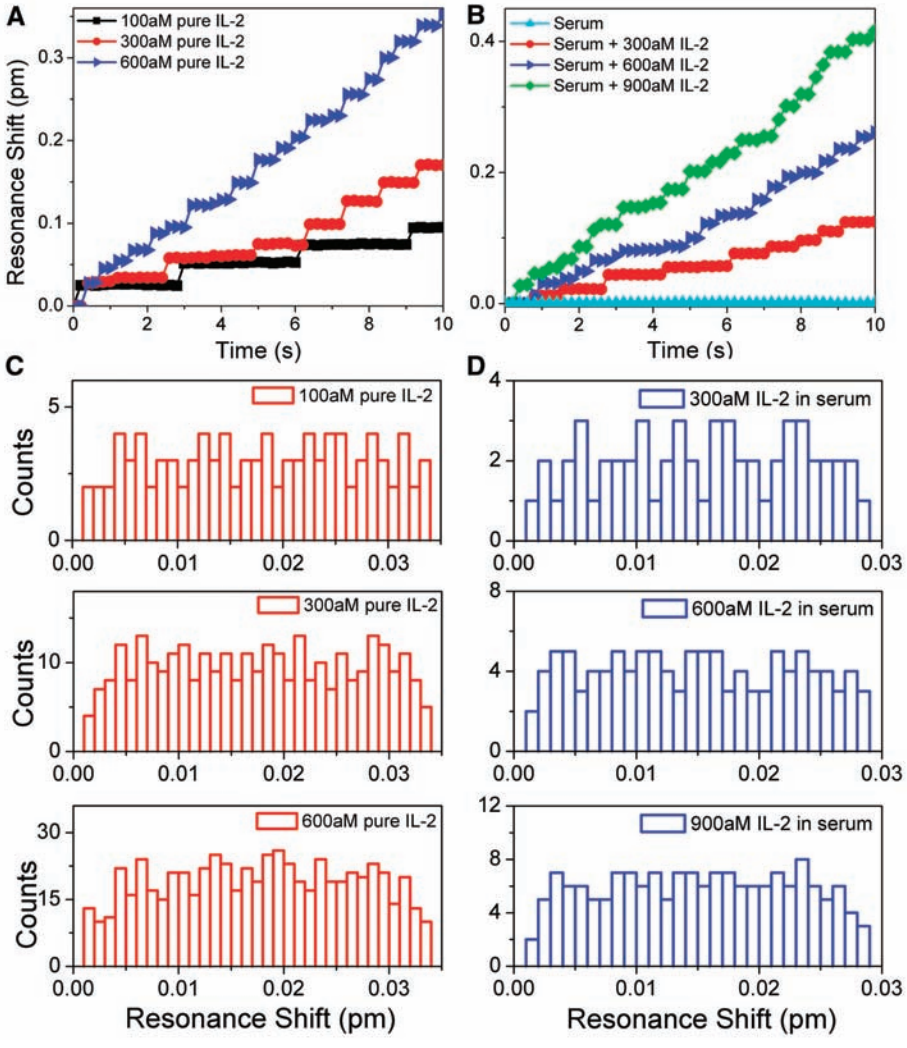

Fig. 3. (**A**) The position of the resonance wavelength as a function of time at three different interleukin-2 concentrations. As molecules bind to the surface, the resonant wavelength position jumps, creating the steps seen. When the concentration is increased, the general slope of the trace increased because the binding rate increased. It is important to note that discrete binding events can be resolved at this data acquisition rate. (**B**) The position of the resonance wavelength as a function of time at three different IL-2 concentrations in fetal bovine serum. Also shown is the case of pure serum. As molecules bind to the surface, the resonant wavelength position shifted, creating the steps seen. Similar to the data shown in (A), the slope is related to the concentration, and individual events are resolved. (**C**) A series of histograms formed from steps like those in (A), showing the relation between total resonant wavelength shift and number of molecules that bound to the surface of the toroid. As the concentration increased, the number of binding events increased; however, the largest shift remained constant. This shift is a result of molecules binding at the highest intensity region on the surface of the toroid. The largest shift achieved agrees very well with the expected shift from the thermo-optic theory based on the Q factor of the microcavity used in this experiment (1.20×10^8). This histogram is formed from 5 min of data, and the bin size is 0.001 pm. (**D**) Histogram showing single-molecule binding events like those in (C). Two features are noteworthy: The largest shift is independent of concentration, and the number of binding events increases in proportion to concentration. The largest shift achieved agrees very well with the expected shift from the thermo-optic theory based on the Q factor of the microcavity used in this experiment (1.05×10^8). This histogram is formed from 1 min of data, and the bin size is 0.001 pm.

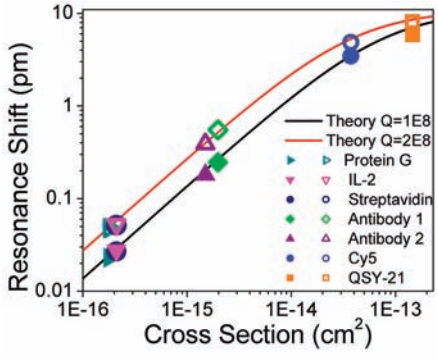

Fig. 4. The expected theoretical relation between absorption cross section and maximum resonance shift is confirmed experimentally for IL-2, streptavidin, protein G, two different IL-2 antibodies, and two synthetic fluorophores (Cy5 and QSY-21). These shifts are determined using the method described in (*26*). The solid symbols were taken using microresonators with $Q \sim 1 \times 10^8$; the hollow symbols were taken using microresonators with $Q \sim 2 \times 10^8$. The two solid curves are the theoretically predicted dependence based on Eq. 1.

largest measured single-molecule resonance shift versus absorption cross section. For small cross sections (that do not lower cavity Q), a linear dependence is expected based on the thermo-optic model presented above (we assume a negligible impact of the size parameter ε). The coupled input power and toroid diameter were constant throughout the measurements. With the exception of the shift data for QSY-21, single-molecule data were obtained for multiple binding events on a single toroid. QSY-21 appreciably lowers the Q factor, which made multiple single-molecule measurements untenable. From Fig. 4, it is apparent that there is excellent alignment of the data across all of the distinct molecules and for both Q factors. Furthermore, it should be noted that the higher Q factor provides a proportionally larger shift, as expected from the proposed mechanism. The solid lines in Fig. 4 are the theoretical predictions based on the previously outlined thermo-optic model, using a single ε value of 35 nm.

The detection mechanism is not purely linear in cross section because a single molecule that is highly absorbing can decrease the cavity Q factor (*26*). This phenomenon occurs both with Cy5 and QSY-21, which impact the Q factor even at the single-molecule level. Because the Q factor is decreased, the circulating intensity is reduced, and the thermo-optic induced heating is also decreased. Thus, the linear fit for smaller cross section molecules (which assumes a constant Q and hence constant circulating power) is expected to break down in these cases in precisely the manner observed.

To verify the application of the microtoroid sensor as a diagnostic tool for medical applications, detection of IL-2 in fetal bovine serum was chosen. As mentioned previously, IL-2 is a cytokine which is released in response to immune system activation. However, the concentration of IL-2 in serum has been shown to change in patients with childhood leukemia and to be an indicator of an impaired immune system (*36*). However, IL-2 is present at very low concentrations (10^{-12} to 10^{-15} M) and, therefore, it can be difficult to detect these changes quickly.

To demonstrate detection of IL-2 in serum, three serum solutions were made that contained 300 aM, 600 aM, or 900 aM of IL-2 (*26*). Additionally, pure serum was flowed over the functionalized toroid (*26*). Figure 3B shows the resonant wavelength shifts that resulted from these detection events. Several features of this data are significant. First, the total resonant wavelength shift increases as a direct function of the concentration, and the individual binding events can be resolved, as in the previous detection events in pure solution (Fig. 3A). Second, the shift from the pure serum is negligible, which indicates that none of the additional components in the serum interferes appreciably with the detection (*26*).

From this resonant shift data, a histogram is created for each of the IL-2 concentrations. Figure 3D shows the distribution of wavelength shifts for all of the single-molecule binding events. The largest shift that occurred (which, as noted before, corresponds to binding at the highest intensity region of the microtoroid) was the same at all three IL-2 concentrations. This value agrees very well with the theoretically predicted value based on the cavity Q for the toroid used in this experiment and the absorption cross section of IL-2. Additionally, the number of molecules that bind increases as a function of the concentration, as would be expected (*26*).

Although there are many other single-molecule detection schemes possible, this UHQ optical microcavity does not require specific labeling of the analyte or antigen in question. This method of detection functions at room temperature and is capable of performing both label-free single-molecule measurements and higher concentration measurements on a single platform. It will enable a new class of biological experiments, including monitoring growth factors that are emitted from living cells in vivo. Because our device is biocompatible and can operate in aqueous environments, it can be used for direct detection of proteins within biological samples without labeling, or even separation, and it should be applicable for the detection of tumor markers present at low concentration in a serum sample or rare growth factors secreted from cells in culture.

References and Notes

1. B. Schuler, E. A. Lipman, W. A. Eaton, *Nature* **419**, 743 (2002).
2. Y. Sako, S. Minoghchi, T. Yanagida, *Nat. Cell Biol.* **2**, 168 (2000).
3. J. K. Jaiswal, S. M. Simon, *Nat. Chem. Biol.* **3**, 92 (2007).
4. M. J. Lang, P. M. Fordyce, A. M. Engh, K. C. Neuman, S. M. Block, *Nat. Methods* **1**, 133 (2004).
5. B. Huang *et al.*, *Science* **315**, 81 (2007).
6. J. Elf, G. W. Li, X. S. Xie, *Science* **316**, 1191 (2007).
7. R. P. Kulkarni, K. Castelino, A. Majumdar, S. E. Fraser, *Biophys. J.* **90**, L42 (2006).
8. B. D. Moore *et al.*, *Nat. Biotechnol.* **22**, 1133 (2004).
9. T. Funatsu, Y. Harada, M. Tokunaga, K. Saito, T. Yanagida, *Nature* **374**, 555 (1995).
10. W. P. Ambrose *et al.*, *Chem. Rev.* **99**, 2929 (1999).
11. S. Myong, I. Rasnik, C. Joo, T. M. Lohman, T. Ha, *Nature* **437**, 1321 (2005).
12. Y. W. C. Cao, R. C. Jin, C. A. Mirkin, *Science* **297**, 1536 (2002).
13. R. C. Hughes, A. J. Ricco, M. A. Butler, S. J. Martin, *Science* **254**, 74 (1991).
14. Z. H. Zhong, D. L. Wang, Y. Cui, M. W. Bockrath, C. M. Lieber, *Science* **302**, 1377 (2003).
15. J. M. Nam, C. S. Thaxton, C. A. Mirkin, *Science* **301**, 1884 (2003).
16. W. S. Yeo, D. H. Min, R. W. Hsieh, G. L. Greene, M. Mrksich, *Angew. Chem. Int. Ed.* **44**, 5480 (2005).
17. T. P. Burg *et al.*, *Nature* **446**, 1066 (2007).
18. S. Arnold, M. Khoshsima, I. Teraoka, S. Holler, F. Vollmer, *Opt. Lett.* **28**, 272 (2003).
19. R. W. Boyd, J. E. Heebner, *Appl. Opt.* **40**, 5742 (2001).
20. E. Krioukov, D. J. W. Klunder, A. Driessen, J. Dreve, C. Otto, *Opt. Lett.* **27**, 512 (2002).
21. A. Ksendzov, Y. Lin, *Opt. Lett.* **30**, 3344 (2005).
22. It is possible to perform single-molecule detection without first sensitizing the surface. This type of detection is shown in Fig. 4 where single-molecule detection experiments of Protein G and QSY-21 were successfully demonstrated without first sensitizing the surface. However, this type of detection has limited applications in biology because specificity is often as important as sensitivity. This surface sensitization is distinct from a label because the antibody is attached to the surface of the microtoroid and not to the molecule of interest (e.g., antigen or streptavidin), whereas a label is attached to the molecule of interest.
23. R. A. Vijayendran, D. E. Leckband, *Anal. Chem.* **73**, 471 (2001).
24. D. K. Armani, T. J. Kippenberg, S. M. Spillane, K. J. Vahala, *Nature* **421**, 925 (2003).
25. A. M. Armani, D. K. Armani, B. Min, K. J. Vahala, S. M. Spillane, *Appl. Phys. Lett.* **87**, 151118 (2005).
26. Materials and methods are available as supporting material on *Science* Online.
27. K. Nakatani, S. Sando, I. Saito, *Nat. Biotechnol.* **19**, 51 (2001).
28. G. F. Zheng, F. Patolsky, Y. Cui, W. U. Wang, C. M. Lieber, *Nat. Biotechnol.* **23**, 1294 (2005).
29. G. H. Wu *et al.*, *Nat. Biotechnol.* **19**, 856 (2001).
30. Turner BioSystems, www.turnerbiosystems.com.
31. E. Fureder-Kitzmuller, J. Hesse, A. Ebner, H. J. Gruber, G. J. Schutz, *Chem. Phys. Lett.* **404**, 13 (2005).
32. The majority of the optical field intensity (over 90%) resides within the toroidal boundary. This fact and the similar magnitudes of the thermal conductivity of water and silica (0.6 and 1.38 W/mK) make it possible to attribute all thermal tuning in (*1*) (and, indeed, the shape of the thermal plume) to the silica. The resulting error in the calculated tuning shift is estimated to be about 5%. We also note that the indicated shift is in steady state, and the response time of the system is set by the thermal response (on the order of microseconds).
33. The actual form of the temperature plume in the vicinity of the molecule is likely complex and has been combined into a single empirical parameter ε. In contrasting a perfect point source of heat with a molecule, this parameter captures the essential fact that the temperature profile is not singular at the source and instead rises steadily until reaching some radius on the order of the molecular size. This approximation is justified, first, because the thermal transport process itself rapidly smoothes nanoscale spatial variations created by molecular shape and, second, because the ensuing temperature field created by the molecular hot spot is long-range (i.e., $1/r$ dependence). For this reason, the tuning shift is only a weak function of the parameter ε. Along these lines, it is the optical cross section σ, as opposed to the physical radius ε, that is of far greater relevance to the thermal-induced tuning. However, the size of ε strongly suggests a maximum temperature in the vicinity of the molecule; therefore, on physical grounds (i.e., molecules are not denaturing in the present work), we expect ε to be many times the actual physical size of the molecule.
34. A cavity linewidth measurement is the minimum sensitivity measurement that can be performed without requiring additional equipment or employing more complex techniques (such as locking onto the resonant wavelength). The primary assumption in this measurement is that the resonant wavelength shifts an entire linewidth upon the binding of a molecule. For example, a cavity with a Q of 100 million operating at 680 nm would need to shift 6.8×10^{-6} nm. As mentioned, this limit is not fundamental but can be viewed as what is detectable by methods that do not enable detection of sub-linewidth shifts. Thus, this limit is the most desirable one to consider when balancing detection limits and experimental complexity.
35. The absorption cross sections of the IL-2, protein G, streptavidin, and the two different IL-2 antibodies were determined with an ultraviolet-visible spectrophotometer (Shimadzu BioSpec-1601, San Diego, CA, USA), whereas the absorption cross section of the Cy5-labeled antibody and the QSY-21 quencher were determined from absorption spectra available from the manufacturer (Invitrogen, Carlsbad, CA, USA). The absorption spectra of the Cy5-labeled antibody and of the bleached Cy5-labeled antibody were verified with the spectrophotometer.

36. B. Mazur, A. Mertas, D. Sonta-Jakimczyk, T. Szczepanski, A. Janik-Moszant, *Hematological Oncology* **22**, 27 (2004).
37. We thank O. Painter for useful discussions, B. Min for FEMLAB simulations, N. Pierce for spectrophotometer measurements, and D. Armani for microtoroid fabrication. A.M.A. is supported by the Clare Boothe Luce Postdoctoral Fellowship. This work was supported by the Defense Advanced Research Projects Agency's Center for OptoFluidic Integration and the Biological Imaging Center of the Beckman Institute at the California Institute of Technology.

Supporting Online Material
www.sciencemag.org/cgi/content/full/1145002/DC1
Materials and Methods
Figs. S1 to S11
References

11 May 2007; accepted 14 June 2007
Published online 5 July 2007;
10.1126/science.1145002
Include this information when citing this paper.

Ultrafast Flash Thermal Conductance of Molecular Chains

Zhaohui Wang,[1]* Jeffrey A. Carter,[1]* Alexei Lagutchev,[1]* Yee Kan Koh,[2] Nak-Hyun Seong,[1]* David G. Cahill,[2,3] Dana D. Dlott[1,3]†

At the level of individual molecules, familiar concepts of heat transport no longer apply. When large amounts of heat are transported through a molecule, a crucial process in molecular electronic devices, energy is carried by discrete molecular vibrational excitations. We studied heat transport through self-assembled monolayers of long-chain hydrocarbon molecules anchored to a gold substrate by ultrafast heating of the gold with a femtosecond laser pulse. When the heat reached the methyl groups at the chain ends, a nonlinear coherent vibrational spectroscopy technique detected the resulting thermally induced disorder. The flow of heat into the chains was limited by the interface conductance. The leading edge of the heat burst traveled ballistically along the chains at a velocity of 1 kilometer per second. The molecular conductance per chain was 50 picowatts per kelvin.

Heat transport is central to the operation of mechanical and electronic machinery, but at the level of individual molecules, the familiar concepts of heat diffusion by phonons in bulk materials no longer apply. Heat is transported through a molecule by discrete molecular vibrations. An emerging area in which vibrational energy transfer becomes crucial is the field of molecular electronics, where long-chain molecules attached to tiny electrodes are used to transport and switch electrons. When an electron is transported through a molecule, a portion of the electron's kinetic energy can be lost, appearing as molecular vibrational energy (*1*). In studies such as this one, in which molecular energy levels are not individually resolved, it is conventional to call such processes "heat dissipation" or "nanoscale thermal transport" (*2*), even though an equilibrium Boltzmann distribution is not necessarily achieved. Nitzan and co-workers (*3*) have estimated that 10 to 50% of the electron energies could be converted to heat, so that a power of 10^{11} eV/s may be dissipated on a molecular electronic bridge carrying 10 nA under a bias of 1 eV. Using classical and quantum mechanical methods, they and others (*1*) have calculated steady-state temperatures resulting from such dissipation. Steady-state calculations, however, do not entirely capture the essence of this phenomenon. The energy lost when electrons are transported through a molecular wire in a fraction of a picosecond appears as staccato bursts, up to 1 eV per burst. On a 10-carbon alkane molecule, for instance, 1eV is enough energy to produce a transient temperature jump $\Delta T \approx 225$ K. At the temperatures associated with these ultrafast energy bursts, Nitzan and co-workers (*3*) suggest that, instead of the usual phonon mechanisms prevalent in ordinary thermal conduction processes (*1*), much of the heat is carried by higher-energy molecular vibrations such as carbon-carbon bending and stretching and carbon-hydrogen bending, which are delocalized over a few carbon segments (*3*).

To study molecular energy transport in the regime of short distances, short time intervals, and large temperature bursts, we have used an ultrafast flash thermal conductance apparatus to study densely packed self-assembled monolayers (SAMs) of long-chain hydrocarbon molecules anchored to metal substrates. Laser flash-heating increased the temperature of the metal substrate to ~800°C in 1 ps. Heat flowed from the metal layer into the base of the molecular chains and then through the chains. A vibrational spectroscopy method was used that selectively probed the thermal-induced disorder of the methyl groups at the ends of the chains. The alkane chain lengths yielded a ballistic velocity for heat flow through the chains, and the measured thermal conductance plus the area per chain yielded a molecular thermal conductance.

The concept of the thermal conductance apparatus is illustrated in Fig. 1A. A femtosecond laser pulse flash-heated an ~300-μm-diameter region of an Au layer crafted for a fast time response of ~1 ps. The SAMs were formed from *n*-alkanethiol molecules HS-$(CH_2)_n$-CH_3 with an even number of carbon atoms from C6 to C24 (i.e., *n* from 5 to 23). A nonlinear coherent spectroscopic method (*4*) termed broadband multiplex vibrational sum-frequency generation spectroscopy (SFG) probed an ensemble of $\sim 10^{11}$ alkane chains at the center of the heated region. We determined an overall rate for heat transport from Au into the alkane chains, and a

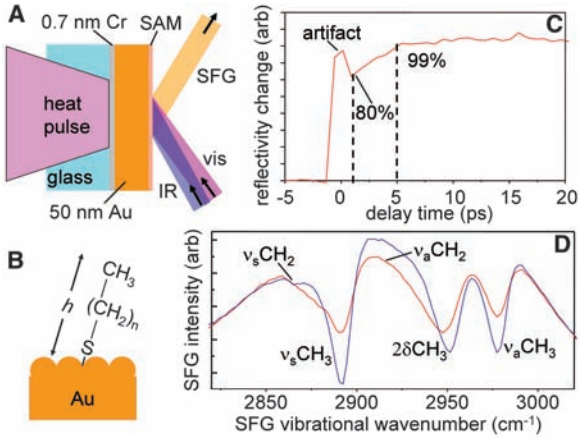

Fig. 1. (**A**) Concept of the ultrafast flash thermal conductance measurements. IR and visible pulses combine to generate SFG in an ~200-μm-diameter region containing ~10^{11} alkane chains. SFG is sensitive to thermal disordering of the alkane terminal methyl groups of SAMs, which occurs when heat propagates from the Au surface to the ends of the alkane chains. (**B**) Alkanethiol molecule of length *h* bound to Au surface. (**C**) Ultrafast thermal reflectance measurements show that the Au layer heats up to 80% of its final temperature in 1 ps. (**D**) SFG spectra of alkane thiol (n = 17) SAM at ambient temperature (blue) and after an ultrafast temperature increase to 800°C (red).

[1]School of Chemical Sciences, University of Illinois at Urbana-Champaign, Urbana, IL 61801, USA. [2]Department of Materials Science and Engineering, University of Illinois at Urbana-Champaign, Urbana, IL 61801, USA. [3]Fredrick Seitz Materials Research Laboratory, University of Illinois at Urbana-Champaign, Urbana, IL 61801, USA.

*These authors contributed equally to this work.
†To whom correspondence should be addressed. E-mail: dlott@scs.uiuc.edu